COBEM 2023 27TH INTERNATIONAL CONGRESS OF MECHANICAL ENGENEERING

ABCM Brazilian Society of Mechanical Sciences and Engineering
27th ABCM International Congress of Mechanical Engineering
December 04-08, 2023, Florianópolis-SC, Brazil

COB-2023-0734
ANALYSIS OF THE CAVITATION EFFECT ON THE PERFORMANCE OF A PLAIN JOURNAL BEARING USING COMPUTATIONAL FLUID DYNAMICS

Fernanda F. Rossi
Aldemir Ap. Cavallini Jr
João Marcelo Vedovotto
Franco Barbi
Leonardo Dias da Silva Cabral
Federal University of Uberlândia, School of Mechanical Engineering, Uberlândia, Brazil
fernandarossi95@ufu.br
aacjunior@ufu.br
vedovotto@ufu.br
frcbarbi@gmail.com
leo01@ufu.br

Abstract. *Cavitation is an important phenomenon in hydrodynamic lubrication that considerably affects the performance of journal bearings. In this context, the present work aims to investigate the cavitation effect on the performance of a plain journal bearing using OpenFOAM®, an open-source software for Computational Fluid Dynamics (CFD) based on the Finite Volume Method (FVM). The results obtained demonstrated that due to the cavitation effect, the pressures in the divergent zone of the bearing cannot be lower than the oil vapor pressure, resulting in an asymmetric pressure distribution and, consequently, a reduction of the load-carrying capacity of the bearing.*

Keywords: *hydrodynamic analysis, cavitation, plain journal bearing, Computational Fluid Dynamics (CFD).*

1. INTRODUCTION

Rotating machinery are mechanical equipment essential in various industrial applications, such as oil and gas, petrochemical, mining, and power generation industries. Bearings are elements responsible for the connection between the moving and stationary parts of a rotating machine, allowing the relative motion between them occurs with minimum friction. Due to its convergent-divergent geometry, cavitation is a phenomenon very common in journal bearings, which causes the lubricant film rupture and directly affects the performance of these components. According to Dowson and Taylor (1979), cavitation can be divided into two types: gaseous cavitation and vaporous cavitation. In gaseous cavitation, the lubricant pressure falls below the saturation pressure, leading to the release of dissolved gases in the fluid and the formation of gas bubbles. On the other hand, if the lubricant pressure continues to decrease until it reaches its vapor pressure, the fluid will start to vaporize, and this process is known as vaporous cavitation.

In recent years, with the development of the high-performance computers and the advance of the numerical methods, Computational Fluid Dynamics (CFD) has become an increasingly popular tool for investigating the performance of hydrodynamic journal bearings. Dhande and Pande (2017) combined CFD and FSI (Fluid-Structure Interaction) techniques to perform an elastohydrodynamic analysis on a journal bearing. Li *et al.* (2019) developed a three-dimensional CFD-CHT (Conjugate Heat Transfer) model to study the temperature distribution within a journal bearing. Yasir *et al.* (2023) used CFD to investigate the impact of nanoparticles on the thermohydrodynamic characteristics of a journal bearing. All these works considered the cavitation effect in modelling.

Even though there is a wide range of commercial CFD software packages available in the market (Ansys CFX®, Ansys Fluent®, COMSOL Multiphysics®), the high cost of these software license fees makes their use unfeasible for the academia. Additionally, the lack of access to the source code of these commercial packages makes it impossible for the users to make changes in it to attend their needs (Ansoni, 2015). In this context, the present work aims to investigate the cavitation effect on the performance of a plain journal bearing using OpenFOAM®, a free open-source software written in C++ that provides a wide range of features to solve problems related to continuum mechanics, with emphasis on CFD.

2. JOURNAL BEARINGS

Plain journal bearings are basically composed of a rotating shaft and a stationary bush separated by a relatively thick film of lubricant that prevents metal-to-metal contact. Due to the rotational motion of the shaft, the lubricant is drawn into

a convergent wedge formed in the bearing clearance, generating a hydrodynamic pressure in the fluid film that is able to separate the sliding surfaces and support the external force acting on the shaft (Dhande and Pande, 2018). Figure 1 shows the schematic representation of this type of bearing, where a circular shaft with a radius of R rotates at a constant angular velocity Ω within a stationary bush with a radius of $R + C_r$ and width L, being the parameter C_r the radial clearance of the bearing. The eccentric position of the journal center O_j relative to the bearing center O_b is defined by the eccentricity e and the attitude angle ϕ.

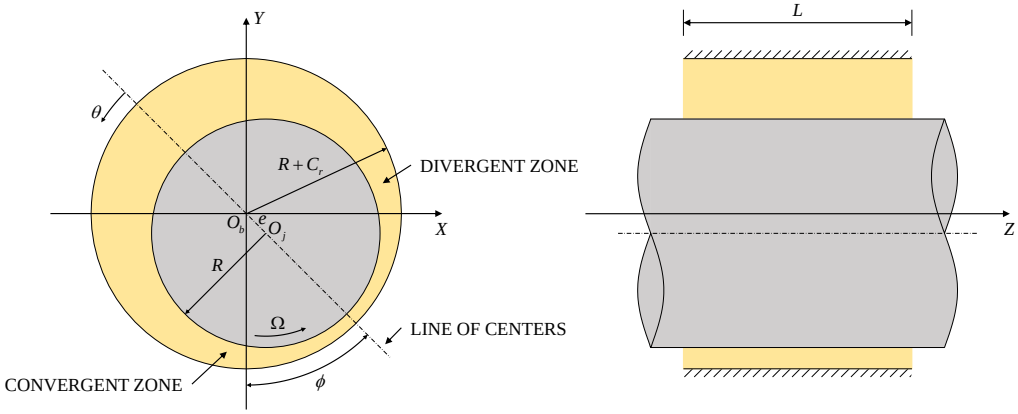

Figure 1: Schematic representation of a plain journal bearing (Dhande and Pande, 2018).

2.1 NUMERICAL ANALYSIS

The isothermal flow of a fluid within a journal bearing is governed by the mass and momentum conservation equations. Assuming that the fluid is a mixture of liquid and vapor, with both phases being treated as incompressible, the continuity and Navier-Stokes equations can be written, respectively, as (Ghahramani *et al.*, 2021):

$$\nabla \cdot \vec{U} = \left(\frac{1}{\rho_l} - \frac{1}{\rho_v}\right) \dot{m}''', \tag{1}$$

$$\frac{\partial \rho \vec{U}}{\partial t} + \nabla \cdot \left(\rho \vec{U} \vec{U}\right) = -\nabla p + \nabla \cdot \left\{\mu \left[\nabla \vec{U} + \left(\nabla \vec{U}\right)^T - \frac{2}{3}\left(\nabla \cdot \vec{U}\right)\mathbf{I}\right]\right\}, \tag{2}$$

where $\vec{U}$ is the mixture velocity vector, $\dot{m}'''$ is the mass transfer rate between the liquid and vapor phases per unit volume, ρ and μ are the density and dynamic viscosity of the mixture, p is the pressure, $\mathbf{I}$ is the identity tensor, and t is the time.

The physical properties of the mixture are defined as:

$$\rho = \alpha \rho_l + (1 - \alpha)\, \rho_v, \tag{3}$$

$$\mu = \alpha \mu_l + (1 - \alpha)\, \mu_v, \tag{4}$$

where α is the liquid volume fraction, and the subscripts l and v refer to the liquid and vapor phases, respectively.

To determine the liquid volume fraction, it is necessary to solve the following transport equation (Ghahramani *et al.*, 2021):

$$\frac{\partial \alpha}{\partial t} + \nabla \cdot \left(\alpha \vec{U}\right) = \frac{\dot{m}'''}{\rho_l}. \tag{5}$$

Since the mass transport occurs due to liquid vaporization or vapor condensation, the mass transfer rate can be expressed as follows:

$$\dot{m}''' = \alpha \dot{m}_v''' + (1 - \alpha)\, \dot{m}_c''', \tag{6}$$

where $\dot{m}_v'''$ and $\dot{m}_c'''$ are the vaporization and condensation rates, respectively.

There are several numerical models that can be used to evaluate the phase change between liquid and vapor, being most of them based on the simplified Rayleigh-Plesset equation for bubble dynamics (Franc, 2007). In this work, the Schnerr-Sauer model will be used to simulate the cavitation in a plain journal bearing. According to this model, the

vaporization and condensation rates are determined by (Ghahramani *et al.*, 2021):

$$\dot{m}_v''' = C_v \left(1 + \alpha_{nuc} - \alpha\right) \frac{3\rho_l \rho_v}{\rho R_B} \sqrt{\frac{2}{3\rho_l \left|p - p_{sat}\right|}} \min\left(p - p_{sat}, 0\right), \tag{7}$$

$$\dot{m}_c''' = C_c \alpha \frac{3\rho_l \rho_v}{\rho R_B} \sqrt{\frac{2}{3\rho_l \left|p - p_{sat}\right|}} \max\left(p - p_{sat}, 0\right), \tag{8}$$

where C_v and C_c are empirical coefficients related to the vaporization and condensation processes, respectively, p_{sat} is the saturation vapor pressure, α_{nuc} is the nucleation site volume fraction, and R_B is the bubble radius. These last two parameters are defined as (Ghahramani *et al.*, 2021):

$$\alpha_{nuc} = \frac{\frac{1}{6}\pi n_0 d_{nuc}^3}{1 + \frac{1}{6}\pi n_0 d_{nuc}^3}, \tag{9}$$

$$R_B = \left(\frac{3}{4\pi n_0} \frac{1 + \alpha_{nuc} - \alpha}{\alpha}\right)^{1/3}, \tag{10}$$

where n_0 is the bubble number density and d_{nuc} is the nucleation site diameter.

3. RESULTS AND DISCUSSION

The geometric and operational characteristics of the plain journal bearing to be studied in this work are presented in Tab. 1. The physical properties of the lubricating oil are listed in Tab. 2.

Table 1: Geometric and operational parameters of the bearing (Wang *et al.*, 2023).

Parameter	**Value**
Shaft radius (mm)	14.97
Bearing width (mm)	20
Radial clearance (mm)	0.03
Eccentricity (mm)	0.018
Atitude angle (°)	45
Rotational speed (rpm)	600

Table 2: Physical properties of the lubricating oil (Wang *et al.*, 2023).

Property	**Value**
Density (kg/m^3)	822 (liquid) 1.29 (vapor)
Dynamic viscosity (Pa·s)	0.014 (liquid) 5.953×10^{-6} (vapor)
Saturation vapor pressure (Pa)	29 185

Figure 2 shows the hexahedral mesh generated in the bearing clearance using OpenFOAM® *blockMesh* utility. Note that the computational domain was divided into $360 \times 100 \times 8$ elements along the circumferential, axial, and radial directions, respectively. The arrangement of these elements along the oil film thickness is depicted in Fig. 3.

The mesh quality can be evaluated based on the parameters presented in Tab. 3. As the oil film thickness is much smaller than the other dimensions of the bearing, the aspect ratio of the mesh elements tends to be high. However, the skewness and non-orthogonality of the elements are low, which improves the mesh quality.

Table 3: Mesh quality parameters.

Parameter	**Value**
Maximum aspect ratio (-)	111.121
Maximum non-orthogonality (°)	10.579
Maximum skewness (-)	0.022

Regarding the boundary conditions, the shaft surface is modeled as a moving wall and the bearing surface as a stationary wall, with the no-slip condition applied at both interfaces. On the bearing sides, the pressure is set equal to

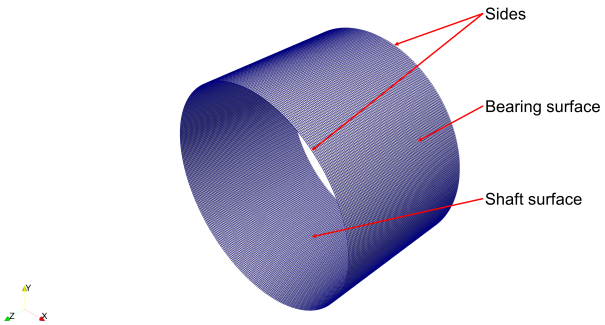

Figure 2: Hexahedral mesh generated in the bearing clearance.

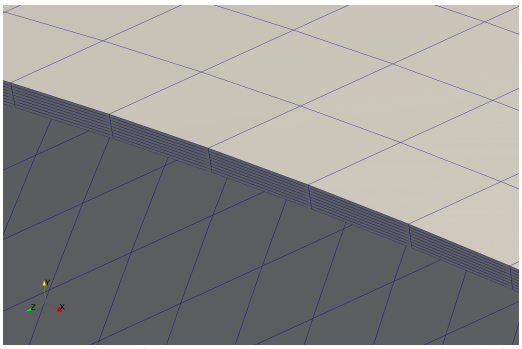

Figure 3: Arrangement of the mesh elements along the oil film thickness.

atmospheric, so that only oil in the liquid phase is present at these boundaries. In summary, Table 4 reports the boundary conditions to be used in the simulation.

Table 4: Boundary conditions.

Boundary	**Pressure**	**Velocity**	**Liquid volume fraction**
Shaft surface	$\partial p/\partial n = 0^{(1)}$	$\vec{\omega} = (0, 0, 62.832)\,\mathrm{rad/s}$	$\partial \alpha/\partial n = 0^{(1)}$
Bearing surface	$\partial p/\partial n = 0^{(1)}$	$\vec{U} = (0, 0, 0)\,\mathrm{m/s}$	$\partial \alpha/\partial n = 0^{(1)}$
Sides	$p = 100\,\mathrm{kPa}$	$\partial \vec{U}/\partial n = 0^{(1)}$	$\alpha = 1$

$^{(1)}$ n is the normal direction to the boundary.

After setting up the case, the transient simulation of the bearing was performed until $0.1\,\mathrm{s}$ using OpenFOAM® solver *interFoam* without taking into account the effects of gravity, surface tension, and interface compression. Figures 4 and 5 illustrate, respectively, the pressure and vapor volume fraction distributions in the oil film at the last time step of the simulation. It is important to note that due to the cavitation effect, the pressures in the divergent zone of the bearing cannot be lower than the oil vapor pressure, resulting in an asymmetric pressure distribution around the position of minimum oil film thickness. Furthermore, the results also indicate that, in contrast to the pressure, the vapor volume fraction changes considerably along the oil film thickness.

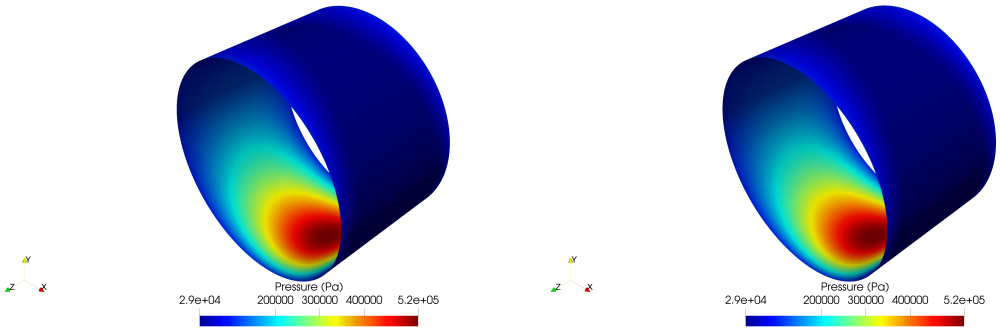

(a) At the shaft surface. (b) At the bearing surface.

Figure 4: Pressure distribution in the oil film.

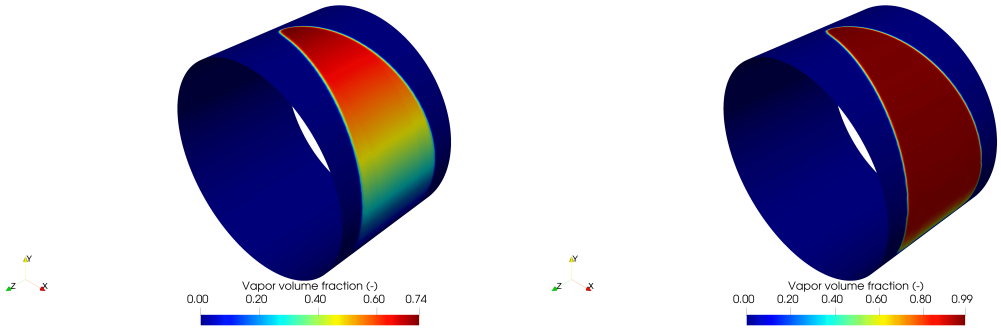

(a) At the shaft surface. (b) At the bearing surface.

Figure 5: Vapor volume fraction distribution in the oil film.

The convergence of the results was verified by monitoring the residuals, hydrodynamic forces, and maximum vapor fraction, as shown in Figs. 6 to 8, respectively. By analyzing these figures, it can be seen that the residuals are low and the oil flow behavior within the bearing is nearly steady after $0.05\,\mathrm{s}$.

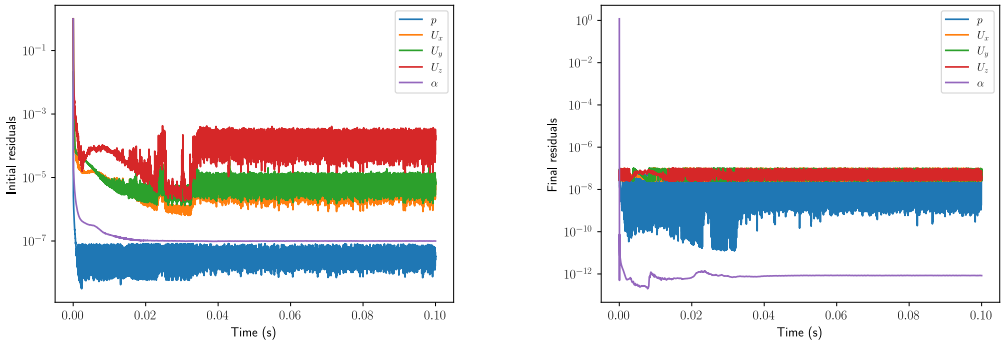

(a) Initial residuals. (b) Final residuals.

Figure 6: Evolution of the residuals during the simulation.

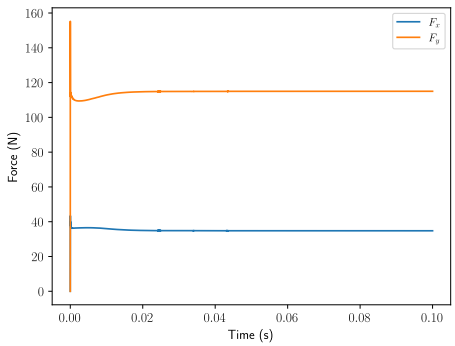

Figure 7: Convergence of the hydrodynamic forces acting on the shaft.

Figure 9 illustrates the cavitation effect on the pressure distribution along the mid-plane of the shaft. From this figure, it can be seen that the maximum pressure in the oil film is underestimated when the cavitation effect is not considered. Additionally, it is observed that in this case, the negative pressures are of the same order of magnitude as the positive pressures. However, since the oil is unable to withstand high tensile stresses without break down, the cavitation effect must be included in the model to ensure that the simulation results are consistent with reality.

4. CONCLUSIONS

In the present work, the cavitation effect was investigated in a plain journal bearing using OpenFOAM®. The results obtained demonstrated that if the lubricating oil were able to withstand high tensile stresses without break down, the

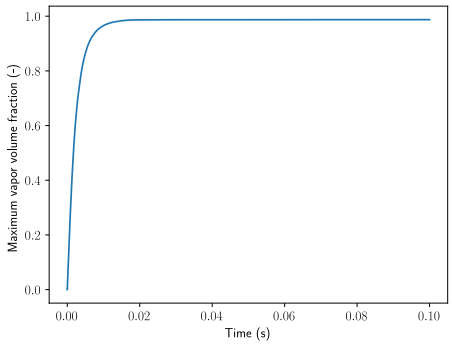

Figure 8: Variation of the maximum vapor fraction in the oil film during the simulation.

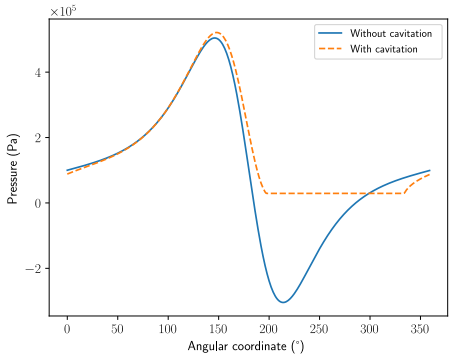

Figure 9: Cavitation effect on the pressure distribution along the mid-plane of the shaft.

pressure distribution in the bearing would be antisymmetric around the position of minimum film thickness, with positive pressures in the convergent region of the clearance and negative pressures in the divergent region. However, due to the cavitation effect, the pressures in the divergent zone of the bearing cannot be lower than the oil vapor pressure, resulting in an asymmetric pressure distribution and, consequently, a reduction of the load-carrying capacity of the bearing.

5. ACKNOWLEDGEMENTS

The authors would like to thank Petrobras for the financial and technical support provided to carry out this research. The authors would also like to acknowledge Prof. Fábio Pereira dos Santos of Federal University of Rio de Janeiro for his help with the numerical simulation.

6. REFERENCES

Ansoni, J.L., 2015. *Methodology for industrial bioreactor design via multiobjective optimization based on performance parameters calculated by CFD techniques (in Portuguese)*. Ph.D. thesis, Universidade de São Paulo, São Carlos.

Dhande, D.Y. and Pande, D.W., 2017. "A two-way FSI analysis of multiphase flow in hydrodynamic journal bearing with cavitation". *Journal of the Brazilian Society of Mechanical Sciences and Engineering*, Vol. 39, p. 3399–3412.

Dhande, D.Y. and Pande, D.W., 2018. "Multiphase flow analysis of hydrodynamic journal bearing using CFD coupled fluid structure interaction considering cavitation". *Journal of King Saud University – Engineering Sciences*, Vol. 30, No. 4, pp. 345–354.

Dowson, D. and Taylor, C.M., 1979. "Cavitation in bearings". *Annual Review of Fluid Mechanics*, Vol. 11, pp. 35–66.

Franc, J.P., 2007. *The Rayleigh-Plesset equation: a simple and powerful tool to understand various aspects of cavitation*, Springer, Vienna, pp. 1–41.

Ghahramani, E., Ström, H. and Bensow, R., 2021. "Numerical simulation and analysis of multi-scale cavitating flows". *Journal of Fluid Mechanics*, Vol. 922, p. A22.

Li, Q., Zhang, S., Wang, Y., Xu, W.W. and Wang, Z., 2019. "Investigations of the three-dimensional temperature field of journal bearings considering conjugate heat transfer and cavitation". *Industrial Lubrication and Tribology*, Vol. 71, No. 1, pp. 109–118.

Wang, Y., Jacobs, G., König, F., Zhang, S. and von Goeldel, S., 2023. "Investigation of microflow effects in textures on hydrodynamic performance of journal bearings using CFD simulations". *Lubricants*, Vol. 11, No. 1, p. 20.

Yasir, M.O., Ahmed, S.Y. and Abass, B.A., 2023. "Performance analysis of experimentally characterized titanium dioxide and zinc oxide nano-lubricated journal bearing considering thermal and cavitation effects". *Arabian Journal for Science and Engineering*, Vol. 48, p. 3599–3614.

7. RESPONSIBILITY NOTICE

The authors are solely responsible for the printed material included in this paper.